Journal of Al-Farabi for Engineering Sciences (JFES)
Vol. 5, No. 1, 2026, **pp**. 14-23
ISSN: 2617-5517 | **DOI**: https://doi.org/10.59746/60dkc389

An Intelligent Deep Residual Network for Automated Lung Cancer Detection Using ResNet50

Zainab Muhammed[1,2] **Belal Al-Khateeb**[3,*]
[1] Informatics Institute for Postgraduate Studies, Information Technology & Communication University, Baghdad,10074, Iraq, e-mail: phd202220704@iips.edu.iq
[2] Computer Science Department, College of Education for Pure Science/ Ibn-Al Haitham, University of Baghdad, Baghdad, 10069, Iraq, e-mail:zainab.m@ihcoedu.uobaghdad.edu.iq
[3] Computer Science Department, College of Computer Science and Information Technology, University of Anbar, Ramadi, 10003, Iraq, e-mail: belal-alkhateeb@uoanbar.edu.iq

Received 20/12/2025, Revised 15/02/2026, Accepted 17/03/2026

Abstract: Lung cancer accounts for one of the leading causes of cancer death in the world; patients' prognosis can be greatly improved when diagnosed and predicted accurately as early as possible. The proposed intelligent deep learning models will enable automatic identification and classification of lung cancer from histopathological images.
The architecture used was a deep residual network based on ResNet-50, trained on approximately 15,000 lung histopathology images in three classes: adenocarcinoma (ACA), squamous cell carcinoma (SCC), and normal tissue (N). Different testing protocols were performed to objectively evaluate the proposed model robustness and generalization capabilities, including prospective tests using images from a single dataset and external tests using images from other sources.
In the experimental results, the overall accuracy for classification using this proposed model was 99.96%, implying a strong classification ability. Additional evaluation with a confusion matrix and ROC curve confirmed the discriminative power of the model, and external testing demonstrated that the model generalized well when tested on unseen samples from different sources.
The findings indicate that the effective ResNet50-based deep learning technique may be employed as a pioneering tool for automatic lung cancer diagnosis, while also supporting pathologists in improving precision and efficiency.

Keywords: Automated Diagnosis, ResNet50, Medical Image Analysis, Lung Cancer, Residual Network.

1. Introduction

Lung cancer ranks as one of the highest annual causes of cancer-related death, claiming millions of lives [1]. The prompt and correct diagnosis is critical for patient survival and effective treatment strategies. The gold standard for both tumor detection and classification are histopathological investigation of the lung biopsied/diseased tissue, which can provide information at the cellular and structural levels. However, histopathology slides are manually analyzed [2] and require large amounts of time-consuming labor, as well as being subject to inter-observer variability that can jeopardize diagnostic reproducibility in medicine [3]. Detecting the presence of a tumor in diagnosing lung cancer is not enough; one must also find out its subtypes, e.g., ACA vs SCC, also. Often, they are highly morphologically similar to each other and cannot be reliably distinguished even by expert/specialist pathologists [4].
Misclassification could lead to inappropriate treatment strategies and, ultimately, impact patient outcomes [5].
On the opposite side, deep learning methods, particularly convolutional neural networks (CNNs), have been advanced and produced promising results for automatic categorization of histopathological images [6-8]. Of these methods, ResNet50 performs remarkably well and introduces a new network structure called residual learning mode that can extract multi-level complex hierarchical features and overcome the problem of gradient disappearance[9]. These models can detect minor morphological differences among tumor subtypes and thereby reduce human error while speeding up the diagnostic workflow[10-12].
But an important challenge remains: the ability of deep learning models to generalize to external datasets [13][14]. Therefore, models that are trained only on a single source can suffer performance drops when applied to images coming from different hospitals/laboratories because of possible differences in the staining procedure, imaging devices, or tissue preparation methods [15-17]. In fact, data in heterogeneous and diverse levels makes automated systems unreliable and lowers their

generalizability when applied to real-world clinical settings, where the use of heterogeneous data sources is common.

While generalization in the sense of diagnosing (detecting) lung cancer and classifying its subtypes from histopathology images is quite best this model will struggle, as it always does, due to indeed extremely high morphological similarity for one dataset versus another that is then compared to external sources: other graphics such as image size/resolution may also prove challenging for network velocity in driving translation efficiencies across domains from one new translational process to another.

This paper contributes to addressing this challenge. This work aims for a ResNet50-based framework and enriches it with basic preprocessing to lessen inter-dataset variability. The backbone is also evaluated on two external tests involving unseen images taken from independent sources, while its ResNet50 component is trained on a large histopathology dataset. This framework exhibits enhanced diagnostic accuracy and stability in differentiating lung cancer subtypes with limited volume of data, indicating its potential to be useful in real, heterogeneous conditions.

Thus, by including sound feature extraction, subtype discrimination, and testing with an external cohort, this study represents a significant step towards the implementation of automated lung cancer diagnosis systems that are capable of being used reliably in different clinical settings.

The remainder of the paper is organized as follows. Related works are presented in Section 2; the proposed method is introduced in Section 3. This is followed by the Results and Discussions in Section 4 and concludes with some recommendations for future work in Section 5.

2. Related Works

In medical image analysis, convolutional neural networks have emerged as a powerful tool for lung cancer detection, leveraging large-scale histopathology image datasets to achieve robust training and validation [18].

In [19], a specialized 9-layer CNN was trained to classify lung tissue (ACA, SCC, and N) using the LC25000 dataset. The model achieves a validation accuracy of 97.2% when trained on histopathology patches of size 180×180 pixels, while training accuracy was 96.11%. The model used on an internal train/test split only, without cross-validation or external dataset validation. This method has significant challenges in overfitting and generalizing the results. Additionally, the architecture of CNN is relatively simple, and this paper does not analyze interpretability or optimizations to work in the real world.

In [20], the authors present a study using a shallow CNN architecture to classify histopathological images obtained from the LC25000 dataset. The classes specifically targeted by the model include benign, adenocarcinoma, and squamous cell carcinoma for lung cancer, and two classes of colon cancer. To solve this, we present a CNN which is made of three convolution and pooling layers specifically optimized to train on image patches while down-sampling, maintaining the textures. The model achieved an accuracy rate of over 97% for lung cancer classification and over 96% for colon cancer classification. The extent of use of the research is limited as cross-validation was not detailed, and external datasets were not used to assess the models, resulting in questions about overfitting and generalizability. Furthermore, the straightforward design of the model architecture and uncertainty about dataset partitioning approaches might influence its robustness in clinical scenarios.

In [21], an ensemble CNN model for classifying three categories of lung tissue, normal, adenocarcinoma, and squamous cell carcinoma, using the LC25000 dataset, was proposed. They utiliz Grad-CAM on the model to also increase explainability, capturing important diagnostic portions of the images. This approach yielded high accuracy results ranging from 97.11% to 99.69%, and AUCs between 99.77% to 99.94%. As a result of the mentioned benefits, another limitation of this study is the absence of external or cross-dataset validation, potentially leading to overfitting or data leakage and increased computational costs due to ensemble learning and visualization techniques.

In [22], residual connections are added to the VGG-19 architecture with preprocessing techniques such as adaptive histogram equalization and CLAHE. Using the three-class lung cancer subset of

the LC25000 dataset (comprised of adenocarcinoma, squamous cell carcinoma, and benign cases), a classification accuracy of 97.73% was achieved by the model. The model performs quite well; much of this performance comes from image augmentations. The limitation of this study is the lack of validation on external datasets or whole-slide images, which raises doubt over its generalizability in clinical applications. Moreover, with the addition of residual blocks, the computational complexity becomes greater than that of the conventional VGG-19 architecture.
In [23], the detection of lung cancer through elaborating deep learning methods was illustrated, and the role of CNNs was particularly emphasized in this study. It used these methods for lung cancer automated classification and prediction in histopathological images, hence reducing reliance on manual assessment. The study uses a large set of histopathological images generated relevant to lung cancer. Train a CNN to identify the patterns associated with types of lung cancer. In the referenced study, the model used achieved an accuracy rate of 95%, which shows that it does an effective job at classifying accurately. The findings showed that the model considerably enhances early detection of lung cancer. The limitations highlighted in this study emphasize the capabilities that advanced computational methods hold for enhancing diagnostic accuracy and efficiency in pathologist-driven processes. Notably, these aspects of methodology, data preprocessing, augmentation techniques, and computational requirements should be further considered. In [24], another study examined the use of ResNet50 architecture. The ResNet50 model has been designed to classify lung cancer into separate classes based on histopathological images. It showcased a high 98% accuracy, highlighting its ability for accurate diagnosis. Thus, it is essential to validate the constructed models externally on several datasets to prove that these models hold utility in real-world scenarios.

3. Methodology

The proposed deep learning framework for lung cancer histopathology classification has been discussed in this section. Figure 1 visualizes the general architecture of the model, listing all important steps of the model.

3.1 Input

The dataset used in the study was derived from [25] and includes histopathological images of lung and colon cancer tissues. Here, only the lung-relevant classes have been used. The dataset has three kinds of classes (lung benign tissue (N), lung adenocarcinoma (ACA), and lung squamous cell carcinoma (SCC). There are 5000 images for each class, thus have 15000 lung images. All images are available in JPEG format, original size: 768 x 768 pixels. The classification tissue in the images acts as labeled data, or ground truth, which aids in training the model and allows different types of lung tissue to be accurately identified.

3.2 Preprocessing

The images, before being used for training, usually go through a preprocessing procedure, which is crucial to make the data more uniform and to increase the performance of the model. That resized all images into 224 × 224 pixels to fit the common deep learning architecture's input size. Normalization of pixel intensity values to a range from 0 to 1 both stabilizes the training process and speeds up model convergence during training, as this improves numerical consistency.

3.3 Setup Hyperparameters

Table 1 shows the model trained for 15 epochs with a stop-early condition to avoid overfitting. To maintain stable gradient updates throughout training, a batch size of 16 was employed. 80% for training and 20% for testing of the dataset. A dropout layer with a rate of 0.25 was used to improve generalization and reduce overfitting. AdamW was the optimizer, and Cross-Entropy Loss served as the objective function for multi-class classification during training. The ReLU activation function was also used to model nonlinearities to encourage feature learning in the network.

 ISSN: 2617-5517 | **DOI**: https://doi.org/10.59746/60dkc389

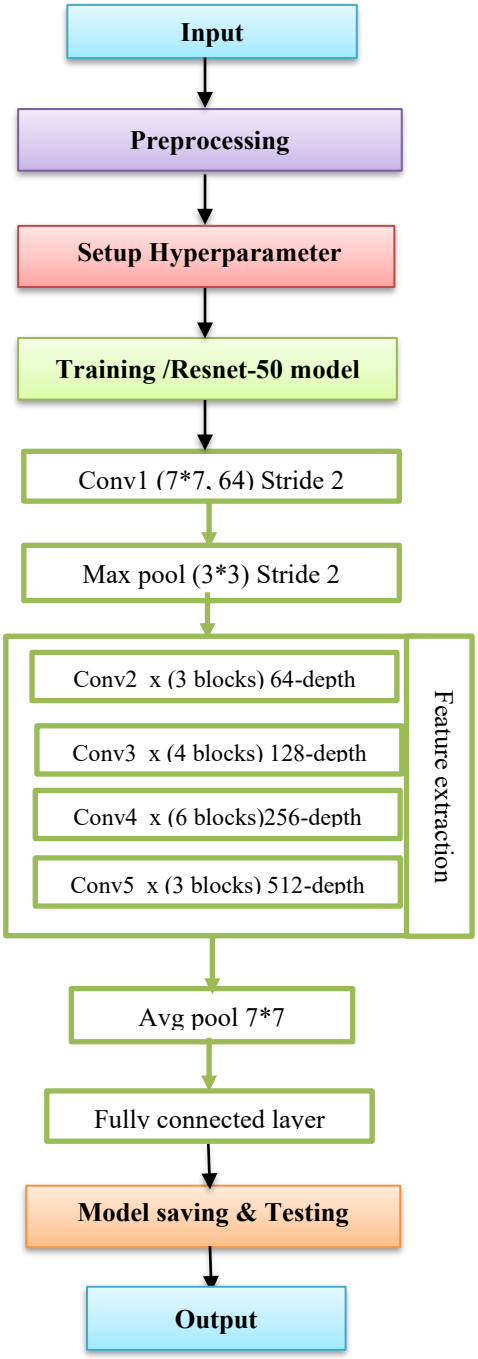

Figure 1. The Proposed Resnet50 Approach

Table 1. Hyperparameter of the proposed approach

Hyperparameter	Value
Epochs	15 epochs with early stop
Dropout Rate	0.25
Batch Size	16
Training Size of Data	80%
Testing the Size of Data	20%
Loss Function	Cross-Entropy Loss
Optimizer	ADAMW
Activation Function	ReLU

3.4 Training with ResNet50

After preprocessing, the normalized images of 224×224-pixel size are fed into the ResNet50 network for training and feature extraction. ResNet50 is a model that contains multiple conv. layers in residual blocks, and the residual connections are used to learn very deep representations, avoiding vanishing gradients.

The input images are first processed by the first convolutional layer (Conv1), which has a kernel size of 7×7 and a stride of two, followed by applying max-pooling to retain meaningful visual information while reducing spatial quantity. This stage is followed by a series of residual convolutional blocks that perform hierarchical feature extraction. There are several convolutional layers organized with 1×1, 3×3, and then again as 1×1 filters. The 1×1 convolution layers enable dimensionality reduction followed by expansion, while the extracted 3×3 convolution layer features capture important spatial patterns from histopathological images. Each successive layer captures hierarchical and abstract representations of the input data, which allows for recognizing subtle details in tissue morphology, cellular structures, or cancer-specific patterns that would otherwise remain undetected with traditional algorithms. Each block has a residual connection that lets each input flow directly to that block's output, aiding in effective gradient propagation for learning features deeper into the network. This process is repeated in the next layer, allowing the network to build high-level features which help it recognize different types of lung.

Finally, the feature maps from the convolutional layers are given to a Global Average Pooling layer, which changes them into a compact feature vector. This vector is then passed to the fully connected layer, where we map learned features to target classes.

Finally, a SoftMax classifier produces probability scores for each of the classes (ACA, SCC, and N) through which the model classifies the input image into one of three categories. At this point in training, the optimizer parameters of the model are adjusted according to the selected loss function and optimizer, to establish a minimum classification error for highly accurate predictions.

3.5 Model Saving & Testing

The model is optimized and then saved so that the performance of learning weights and network parameters can be reused in the future without doing it again. Load the saved model for evaluating or doing inference on new images.

Consider three scenarios for testing:

- Test image previously trained on the dataset (used to condition whether your model learnt correctly).
- Extra test images which come from the same dataset but were not used to train the model, offering a measure of generalization within the same source of data.
- Extra test images obtained from an external source to evaluate the robustness of the trained model on previously unseen images, potentially with different staining, resolution, or acquisition conditions.

All images are pre-processed before testing in the same way as they were for the training data, including the size of input (224 × 224 pixels) and normalization. The images are then transferred to the trained ResNet50 network for feature extraction and classification.

3.6 Output

The model produces a probability score for each class, ACA, SCC, and N per input image. The classes with the highest probability of being the predicted one. This is followed by comparing the predicted output with the actual labels to see if the classification is correct. This enables the computation of performance metrics and the visualization of results, allowing them to clearly visualize how accurately the model can identify each tissue type in multiple testing conditions.

4. Results and Discussion

The proposed deep learning model was trained using a publicly available lung histopathological dataset [25], with three main classes (SCC, ACA, and N) to train the proposed deep learning model. The ResNet50-based deep residual architecture was trained for a maximum of 15 epochs using an early stopping mechanism to prevent overfitting and retain the best

generalization. As indicated in Table 2, the model made a relatively quick approach to convergence at the beginning of training, which reached 90.88% train accuracy and 96.59% test accuracy on epoch one and achieved up to 99.05% by epoch three. There were small fluctuations in epochs 4 and 5, but the model quickly stabilized, with testing accuracy staying above 99% in the following epochs. Over 11 epochs at the best F1 score, we achieved 100% testing accuracy (precision=100%, recall=100%), with a low-test loss of 0.0215. The training and testing performance of the model is depicted through accuracy and loss curves over several epochs. Figure 2 shows that these results demonstrate a very quick drop of the training and testing loss in the early epochs, stabilizing at very low values later, meaning effective learning and overall convergence of the model, both training and testing accuracy steadily grew to 99-100% in the last epochs. The proximity of the training and testing curves indicates that our model generalizes well to unseen data with no clear signs of overfitting. These results indicate the convergence of the training process and the testing of the effectiveness of our model to learn discriminative features from lung cancer data.

Table 2. Proposed Model Results

Epoch	Train Loss	Train Accuracy	Test Loss	Test Accuracy	Test Precision	Test Recall	Test F1-score	Training Time
1	0.2845	90.88%	0.0770	96.59%	97%	97%	97%	1m 47s
2	0.0854	96.36%	0.0583	98.42%	98%	98%	98%	1m 47s
3	0.0619	97.69%	0.0405	99.05%	99%	99%	99%	1m 47s
4	0.0539	98.05%	0.0644	97.65%	98%	98%	98%	1m 48s
5	0.0474	98.59%	0.1912	94.79%	96%	95%	95%	1m 48s
6	0.0467	98.50%	0.0432	99.12%	99%	99%	99%	1m 48s
7	0.0280	99.64%	0.0234	99.93%	100%	100%	100%	1m 48s
8	0.0238	99.89%	0.0231	99.89%	100%	100%	100%	1m 48s
9	0.0230	99.85%	0.0292	99.52%	100%	100%	100%	1m 48s
10	0.0256	99.73%	0.0254	99.82%	100%	100%	100%	1m 48s
11	0.0231	99.85%	0.0215	100.00%	100%	100%	100%	1m 48s
12	0.0235	99.86%	0.0217	99.93%	100%	100%	100%	1m 48s
13	0.0260	99.63%	0.0217	99.96%	100%	100%	100%	1m 48s
14	0.0239	99.76%	0.0253	99.71%	100%	100%	100%	1m 48s
15	0.0211	99.94%	0.0209	99.96%	100%	100%	100%	1m 48s

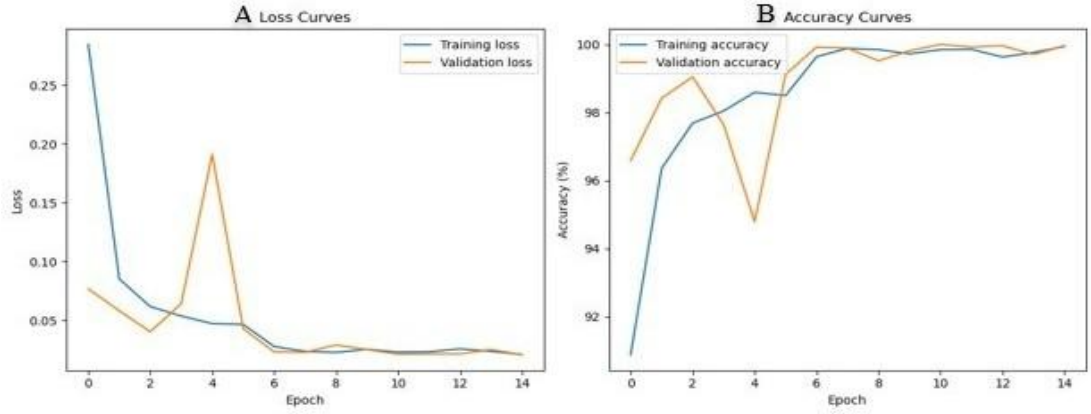

Figure 2. (A)Training and Testing Loss (B) Training and Testing Accuracy

For further evaluation of the generalization capability of the proposed model, additional histopathological images (not included in the training phase) derived from a similar dataset source were used for extra testing. As presented in Table 3, the model successfully recognized 1366 images from a total of 1367 images with an overall accuracy of 99.9% (processing time, 0.23 s per image), achieving a classification rate of SCC and N classes of 100% as well as ACA with an accuracy rate of ~99.7%. Only one misclassification was noted between the cancer classes (SCC and ACA), and this finding could be explained by the similarity of some morphological histopathological aspects, but regarding normal samples, they are always easily differentiated, so only very few errors of classification are obtained.

 ISSN: 2617-5517 | **DOI**: https://doi.org/10.59746/60dkc389

Table 3. Extra Testing Image for the Proposed Model on the same source

Number of images in each class	Number of correctly identified images	Accuracy	Time
scc=449 image	scc=449 image	scc=100%	0.23s
n=580 image	n=580 image	n=100%	
aca=338 image	aca=337 image	aca=99.7%	
1367 images	1366 images	99.9%	

The confusion matrix in Figure 3 indicates that the model demonstrated extremely high classification performance against the supplementary test set. The samples were mostly accurately classified among three classes: ACA, N, and SCC. In detail, the algorithm accurately classified 338 images for ACA, 580 images for N, and 448 images for SCC, with only one misclassification in the SCC class. The performance also indicates the model has the best ability to differentiate between lung tissue categories. Additionally, the Receiver Operating Characteristic curves (ROC) in Figure 4 show good discriminative features for all classes (ACA, N, and SCC), whose AUC value of 1.000 for each class. Notice how close the curves are to the top corner of ROC space, with a near-perfect true positive vs. a very low false-positive rate.

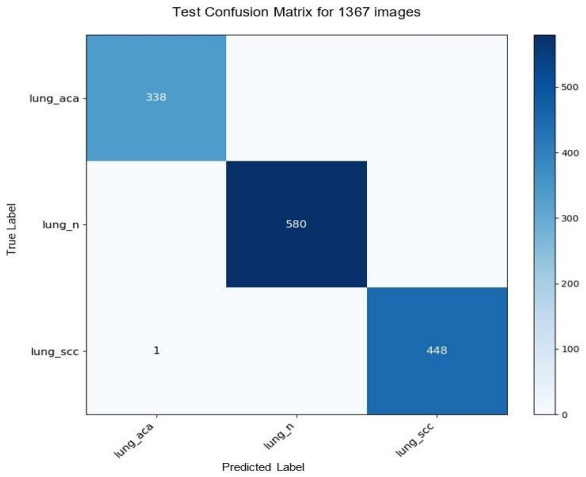

Figure 3. Confusion Matrix for the extra test on the same source

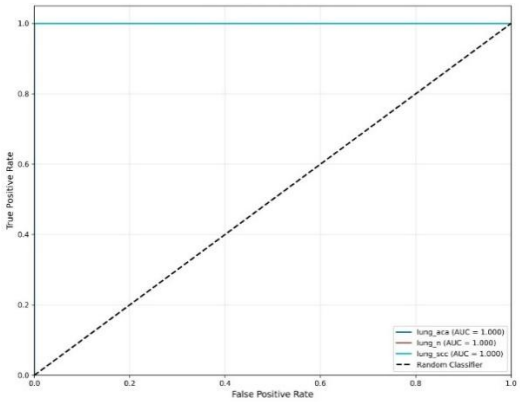

Figure 4. ROC for the extra test on the same source

In addition, the results of additional testing on images taken from another source are shown in Table 4 to illustrate the robustness of the proposed model. The dataset contained 107 images for the three classes (SCC = 54, N = 28, and ACA = 25). The model correctly classified 104 images from the dataset with a total accuracy of 97.4% running in 0.15 s/ image; class-wise performance was also good for SCC (96.2% or 52 images), N (100%, or28images), and ACA (96% or 24

images). These results show that the proposed model retains the best generalization power and excellent performance on images from another data source.

Table 4. Extra Testing Image for the Proposed Model on the other source

Number of images in each class	Number of correctly identified images	Accuracy	Time
scc=54 image	scc=52 image	scc=96.2%	0.15s
n=28 image	n=28image	n=100%	
aca=25 image	aca=24 image	aca= 96 %	
107 images	104 images	97.4%	

The confusion matrix, as shown in Figure. 5, shows the performance of the proposed model on an external test dataset captured from a different source. Such an example shows the Classification results for Images, where most of the images were correctly classified in three categories, namely (ACA, N, and SCC), as shown below, with some misclassified cases also observed. These machine-learning classification errors can be, at least in part, explained because several cancer subtypes share histopathologic features (e.g., ACA vs SCC), and therefore their automated models should determine them not only by their histological features alone. Additionally, the ROC curves depicted in Figure. 6 further validate the excellent discriminative power of our model. The AUC values were excellent for classification performance, being 0.972 in ACA, 0.995 in SCC, and even reaching 1 in N. It shows the maintainability of greater sensitivity and specificity since all curves stick around the best area of the ROC Space. Note that the above results were obtained on images from a data set unseen during training time, suggesting that the proposed model can generalize well and can process data taken from previously unseen sources.

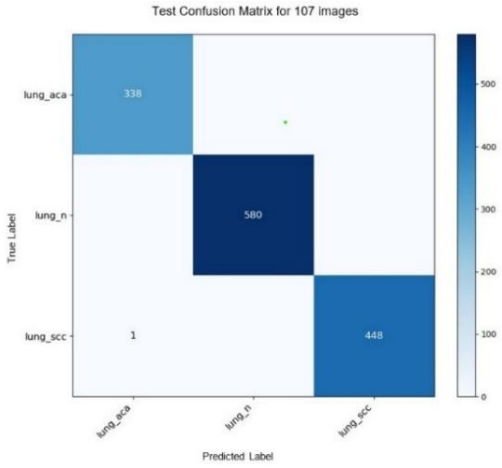

Figure 5. Confusion Matrix for the extra test on the other source

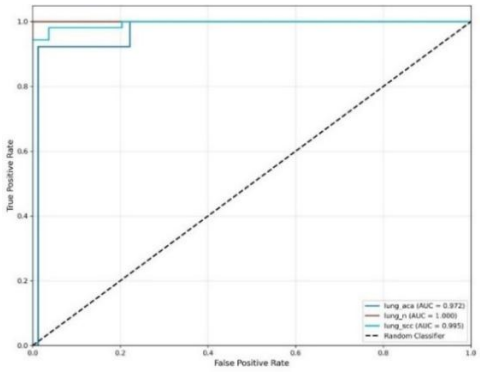

Figure 6. ROC for the extra test on the other source

The comparison of the proposed model is shown in Table 5 together with the previous studies reported in the literature. Most cited works used deep learning models, including custom CNN architectures, shallow CNNs with ensemble and viz techniques, and VGG-19-derived networks that yielded accuracy values ranging from 95.00% to 99.69%. On the contrary, the baseline model based on ResNet50 observed an accuracy of 99.96%. Moreover, the previous work typically used images from the same dataset source to assess their models. In this study, though, further validation was conducted through testing Iraqi clinical images from another dataset to ensure the accuracy of the model. Results show that the proposed model achieves competitive accuracy while also retaining good generalization to data outside of the training source.

Table 5. Comparison with Previous Research

No.	Reference	Method Used	Accuracy Achieved
1	[19]	Custom 9-layer CNN	97.20 %
2	[20]	Shallow 3-layer CNN	97.89 %
3	[21]	Ensemble CNN + Grad-CAM visualization	97.11–99.69 %
4	[22]	Residual VGG-19 + CLAHE	97.73 %
5	[23]	Baseline CNN	95.00 %
6	[24]	Transfer-learned ResNet-50 CNN	98.00 %
8	Proposed Model	Resnet50	99.96%

5. Conclusion

In this study, a deep learning model based on ResNet50 was proposed for classifying lung histopathological images into three classes (ACA, SCC, and N). These experiments revealed that the proposed model (reported accuracy of 99.96%) attained excellent performance on one main test dataset. Further assessment, employing both the same-source images and externally collected Iraqi data set, continued to increase the measure of robustness and generalizability, with AUC values consistently high. These outcomes demonstrate that the suggested solution proves productive in aiding lung cancer subtypes automated discovery and characterization. In future work, the dataset can still be elongated, and more images from other medical centers can be included to achieve higher diversity of the data and further verification of the model's generalization ability. Furthermore, implementing explainable AI approaches and validating the model under real clinical conditions may contribute to enhancing interpretability and supporting its potential use as a diagnostic assistance tool for pathologists.

Funding Information: The authors state no funding is involved.
Authors' Contributions: **[**Zainab Muhammed] designed the methodology, designed the software, performed the experiments, reviewed the collected data, and made the initial analysis and writing. [Belal Al-Khateeb]oversaw the study, developed the research idea, helped interpret the data, facilitated project administration, provided key resources, and approved the final manuscript.
Conflicts of Interest: The authors state no conflict of interest.
Ethical Approval: This study does not involve humans, animals, or sensitive data that require ethical approval.
Data Availability Statements: The datasets and materials supporting this study will be available from the corresponding author on reasonable request.

References

[1] S. Anjum, I. Ahmed, M. Asif, *et al*., "Lung Cancer Classification in Histopathology Images Using Multiresolution Efficient Nets," *Comput. Intell. Neurosci.*, 2023, pp. 1–12, doi: 10.1155/2023/7282944.
[2] M. Chen, "A Comparative Study of Transfer Learning Based Models for Lung Cancer Histopathology Classification," *Highlights Sci. Eng. Technol.*, 2023, pp. 1–8, doi: 10.54097/hset.v39i.6488.
[3] M. M. R. Said, M. S. B. Islam, R. M. Al Saady, *et al*., "Innovative Deep Learning Architecture for the Classification of Lung and Colon Cancer From Histopathology Images," *Appl. Comput. Intell. Soft Comput.*, 2024, pp. 1–18, doi: 10.1155/2024/5562890.
[4] "Automated Classification of Lung Cancer Subtypes Cells Using Microscopic Images and Ensembled Deep Learning Architectures," *Sci. Rep.*, 2025, pp. 1–14, doi: 10.1038/s41598-025-29492-3.

[5] S. Zhong, G. Wang, X. Liao, and S. Zhang, "Segmentation and Classification of Lung Cancer Using Deep Learning Techniques," *Procedia Comput. Sci.*, vol. 235, pp. 3226–3235, 2024, doi: 10.1016/j.procs.2024.04.305.
[6] D. M. Nair, N. M. Shaji, M. B. M., *et al*., "Classification of Lung Cancer from Histopathology Images Using Deep Ensemble Classifier," *Int. J. Res. Appl. Sci. Eng. Technol.*, vol. 14, no. I, pp. 1–7, 2026, doi: 10.22214/ijraset.2026.77154.
[7] F. Al Qahtani, *et al*., "Enhanced Diagnosis of Lung and Colon Cancer through a Deep Learning Ensemble Model," *Diagnostics*, vol. 20, art. 2274, 2024, doi: 10.3390/diagnostics14202274.
[8] S. K. Jha, A. Prakash, and R. Singh, "Automated Lung Cancer Classification from Histopathology Images Using Ensemble Deep Learning Techniques," Biomedical Signal Processing and Control, vol. 88, p. 105654, 2024, doi: 10.1016/j.bspc.2023.105654.
[9] X. Xu, F. Liu, S. Chen, et al., "Deep Learning-Based Classification of Lung Cancer Histopathological Images Using ResNet and DenseNet Architectures," Computers in Biology and Medicine, vol. 166, p. 107512, 2024, doi: 10.1016/j.compbiomed.2023.107512.
[10] Z. Muhammed and B. Al Khateeb, "CNN-EWC: A Continuous Deep Learning Approach for Lung Cancer Classification," *J. Intell. Syst.*, vol. 34, no. 1, pp. 179–201, 2025, doi: 10.1515/jisys-2024-0541.
[11] H. Yang, L. Chen, Z. Cheng, *et al*., "Deep Learning-Based Six-Type Classifier for Lung Cancer and Mimics from Histopathological Whole Slide Images: A Retrospective Study," *BMC Med.*, vol. 19, art. 80, 2021, doi: 10.1186/s12916-021-01953-2.
[12] H. T. Nguyen, Q. H. Tran, and T. T. Le, "Multi-Class Classification of Lung Cancer Subtypes Using Transfer Learning on Histopathological Images," Applied Sciences, vol. 14, no. 3, p. 1452, 2024, doi: 10.3390/app14031452.
[13] R. K. Mishra and S. Tripathi, "Attention-Based Deep Learning Model for Lung Cancer Classification Using Histopathology Images," Expert Systems with Applications, vol. 235, p. 121237, 2024, doi: 10.1016/j.eswa.2023.121237.
[14] D. Roy, S. Banik, and A. Chatterjee, "Explainable Deep Learning Model for Lung Cancer Detection and Classification from Histopathological Images," Diagnostics, vol. 14, no. 2, p. 214, 2024, doi: 10.3390/diagnostics14020214.
[15] W. Li, S. Yu, R. Yang, *et al*., "Machine Learning Model of ResNet50-Ensemble Voting for Malignant-Benign Small Pulmonary Nodule Classification on Computed Tomography Images," *Cancers (Basel)*, vol. 15, no. 22, art. 5417, 2023, doi: 10.3390/cancers15225417.
[16] "Lung Cancer Disease Prediction with CT Scan and Histopathological Images Feature Analysis Using Deep Learning Techniques," *Results Eng.*, vol. 15, art. 101111, 2023, doi: 10.1016/j.rineng.2023.101111.
[17] P. Rajpurkar, E. Park, J. Irvin, et al., "Deep Learning for Chest Cancer Diagnosis: A Comprehensive Review of Histopathology and Imaging Techniques," IEEE Reviews in Biomedical Engineering, vol. 17, pp. 88–102, 2024, doi: 10.1109/RBME.2023.3321456.
[18] S. Anisha D. P. J., *et al*., "Deep Learning Algorithms for Classification of Lung Cancer Types from Histopathological Images," *Int. J. Res. Appl. Sci. Eng. Technol.*, vol. 14, no. I, pp. 12–20, 2026, doi: 10.22214/ijraset. 2026. deep.
[19] M. F. Khatun, M. R. Ajmain, and Md. Assaduzzaman, "A Deep Learning Approach to Detect and Classification of Lung Cancer," in *Proc. ICONAT*, 2023, pp. 1–6, doi: 10.1109/ICONAT57137.2023.10080801.
[20] B. K. Hatuwal and H. C. Thapa, "Lung Cancer Detection Using Convolutional Neural Network on Histopathological Images," *Int. J. Comput. Trends Technol.*, vol. 68, no. 10, pp. 21–24, Oct. 2020, doi: 10.14445/22312803/ijctt-v68i10p104.
[21] S. Mangal, A. Chaurasia, and A. Khajanchi, "Convolution Neural Networks for Diagnosing Colon and Lung Cancer Histopathological Images," *arXiv*, Sep. 2020.
[22] J. Civit-Masot, A. Bañuls-Beaterio, M. Domínguez-Morales, M. Rivas-Pérez, L. Muñoz-Saavedra, and J. M. Rodríguez Corral, "Non-Small Cell Lung Cancer Diagnosis Aid with Histopathological Images Using Explainable Deep Learning Techniques," *Comput. Methods Programs Biomed.*, vol. 226, p. 107108, Nov. 2022, doi: 10.1016/j.cmpb.2022.107108.
[23] S. Wadekar and D. K. Singh, "A Modified Convolutional Neural Network Framework for Categorizing Lung Cell Histopathological Image Based on Residual Network," *Healthcare Analytics*, vol. 4, p. 100224, Dec. 2023, doi: 10.1016/j.health.2023.100224.
[24] R. D. Mohalder, K. A. Hossain, J. P. Sarkar, L. Paul, M. Raihan, and K. H. Talukder, "Lung Cancer Detection from Histopathological Images Using Deep Learning," in *Machine Intelligence and Emerging Technologies*, vol. 490, pp. 201–212, 2023, doi: 10.1007/978-3-031-34619-4_17.
[25] "Lung and Colon Cancer Histopathological Images," *Kaggle*. [Online]. Available: https://www.kaggle.com/datasets/andrewmvd/lung-and-colon-cancer-histopathological-images